Journal Home Page: https://sjes.univsul.edu.iq/

Research Article:

Estimation and Calibration of Hardening Soil Model Parameters for Cohesive Soil Using PLAXIS: A Case Study of Darbandikhan Dam

Alan Ghafoor[1,a,*]
Kawa Zaidan[2,a]
Younis M. Ali[3,b]
[a] University of Sulaimani, College of Engineering, Water Resources Engineering Department
[b] University of Sulaimani, College of Engineering, Civil Engineering Department

Article Information

Article History:
Received : February 11th 2025
Accepted :April 6, 2025
Available online: April , 2025

Keywords:
Hardening Soil Model, HSM, stiffness modulus, PLAXIS, triaxial test.

About the Authors:
Corresponding author:
Alan Ghafoor
E-mail: alan.ghafoor@univsul.edu.iq
Researcher Involved:
kawa.abed@univsul.edu.iq
younis.ali@univsul.edu.iq

DOI https://doi.org/10.17656/sjes.10192

Abstract

This study mainly focuses on identifying and calibrating the Hardening Soil Model HSM parameters for reconstituted soil samples representing the clay core of Darbandikhan Dam. Data from previous investigations and laboratory tests were coupled with numerical modeling to estimate the key parameters, such as stiffness moduli, stress dependency power of stiffness, and shear strength parameters. The reference secant modulus E_{50} was derived from replicated consolidated undrained triaxial tests at different confining pressures using PLAXIS, with a calibrated value of E_{50}^{ref} = 3100 kN/m². Oedometer stiffness E_{oed} was estimated from one-dimensional consolidation tests under different density and moisture content conditions, yielding a reference modulus of 3320 kN/m². Key findings indicate significant variability in soil stiffness and stress dependency, with a stiffness exponent *(m)* ranging from 0.66 to 0.80, influenced strongly by initial density and moisture content. The friction angle (φ) was calibrated to 25°, aligning closely with historical data. Finally, the simulated results based on the parameters numerically calibrated against undrained triaxial tests using PLAXIS finite element software showed strong agreement with the laboratory results.

1. Introduction

The Darabandikhan Dam, a zoned rockfill dam, is a critical water resource structure consisting of various zones of soil types and occupied by several auxiliary structures serving operational purposes. The core zone consists of fine-grained soil, with dominant clay content. The clay zone acts as a water tight barrier to control water seepage. This zone occupies only a narrow strip of the dam section, it cannot withstand high hydraulic pressure of the standing water behind the dam. To mitigate this, the core is supported by upstream and downstream shell of sluiced dumped rock. Chimney filters were provided at upstream and downstream interfaces between the shell and core zones to manage seepage, and reduce soil particle migration. The dam's ancillary structures, including the spillway, bottom outlets, grouting tunnel, and powerplant establishment, are primarily constructed from concrete. The entire dam assemblies including the dam body and the ancillary structures lies on a bedrock of various formations and mechanical properties. Since its construction in the late1950s, the Darbandikhan Dam has been extensively studied. The related technical reports are available within the historical archive of the dam, including (Analyses and Safety Evaluation, Appendix B, 1987; Blanc, 1963a, 1963b; Coyne and Bellier, 1978; Davis, 1958; SMEC International Pty. Ltd., 2006; Wermelinger, 2000). Following the 2017 Mw 7.3 Halabja earthquake the researches have focused on the assessment of the damage caused by the earthquake (Abdullah et al., 2020; Saed et al., 2022; Yousif et al., 2019; Zaidan et al., 2021) and the stability of the dam body and abutments (Al-Husseinawi et al., 2018; AL-Rahal et al., 2020; Mahdi, 2021; Mollamahmutoglu & Bedirhanoglu, 2019; Salim & Noori, 2021; Sissakian et al., 2018). Furthermore, several researchers targeted other aspects of this major event from seismology perspectives (Al-Taie & Albusoda, 2019; Huang et al., 2019; Ibrahim et al., in review; Naserieh et al., 2022; Saed et al., 2022; Yaghmaei-Sabegh, 2019). Nonetheless, there have been few attempts to use numerical methods to model different situations pertaining to the dam's safety during regular operation

or when significant risk presents, for instance, after strong earth motion (AL-Rahal et al., 2020; CREA Hyrdo & Energy, 2022; Mahdi, 2021; Mollamahmutoglu & Bedirhanoglu, 2019; Salim & Noori, 2021). Despite these efforts, many studies relied on simplified soil models like Mohr-Coulomb, which cannot fully capture the non-linear, stress-dependent behavior of soils. Some limitations of these models underscores the need for robust soil models and calibrated parameters. The aim of this study is to derive and calibrate the Hardening Soil Model (HSM) parameters for the Darbandikhan Dam's clay core. The Hardening Soil Model, an advanced constitutive soil model, offers significant improvements in predicting soil behavior compared to traditional methods. It incorporates key features such as stress-dependent stiffness, shear and volumetric hardening, and non-linear stress-strain relationships, making it particularly suitable for analyzing the performance of earth dams under various loading conditions. Despite its advantages, the application of the HSM to the Darbandikhan Dam has been limited, primarily due to challenges in accurately determining the required input parameters. Previous studies have often used estimated or uncalibrated parameters, resulting in reduced reliability of numerical predictions.

To obtain the necessary soil properties and parameters, we adopted four approaches explained as follows:

1. Retrieving relevant data from available field and laboratory test results within the archive of Darbandikhan Dam.
2. Performing laboratory tests on clay core samples to determine required soil parameters or confirm an available one.
3. Manipulating soil correlations to drive soil parameters from apparent soil properties based on established procedures.
4. Calibration of soil parameters based on the Hardening Soil model using a numerical approach imbedded in PLAXIS software.

By combining historical data, laboratory testing, and advanced modeling techniques, this study addresses these gaps, providing calibrated HSM parameters that accurately represent the clay core's behavior.

2. The Hardening Soil Model

For both sandy soils, clays and silts, the Hardening Soil Model accurately depicts several characteristics of actual soil behavior. This advanced hyperbolic soil model was created with the framework of hardening plasticity. It has a yield cap, beyond which the soil acts as a completely plastic material, and it models soil dilatancy by using the theory of plasticity rather than the theory of elasticity to simulate soil hardening. The model also supersedes the well-known former pseudo-plastic (i.e. hypo-elastic) model of Duncan-Chang due to its capacity to differentiate between loading and unloading conditions and its applicability for calculating collapse loads in the completely plastic range (Schanz et al., 1999). Furthermore, this model is based on the Mohr-Coulomb (M-C) failure criterion and contains two main types of hardening, namely shear hardening and volumetric hardening. Shear hardening is used to model irreversible strains due to primary deviatoric loading. Compression hardening is used to model irreversible plastic strains due to primary compression in oedometer loading and isotropic loading. The basic idea for the formulation of the HSM is the hyperbolic relationship between axial strain ε_1, and deviatoric stress q as suggested by Kondner & Zelasko (1963). According to this model, the hyperbolic relationships of standard drained triaxial tests tend to yield curves, which can be described by Equation1:

$$\varepsilon_1 = \varepsilon_1^e + \varepsilon_1^p = \frac{q}{E_{ur}} + \frac{1}{2}\left(\frac{q_a}{E_{50}}\frac{q}{q_a - q} - \frac{2q}{E_{ur}}\right) = \frac{q_a}{2E_{50}}\frac{q}{q_a - q} \quad \dots (1)$$

ε_1 is the total strain; ε_1^e is the elastic strain; ε_1^p is the plastic strain; q is the deviatoric stress; E_{ur} is the unloading/reloading modulus; q_a asymptotic stress; E_{50} is the secant modulus at 50% of the failure stress. Equation 1 essentially combines both elastic and plastic components of strain, reflecting how soil deforms under loading and incorporates parameters that account for the material's stiffness and hardening behavior.

The parameter E_{50} can be related to reference secant modulus E_{50}^{ref} through the Equation 2.

$$E_{50} = E_{50}^{\text{ref}} \left(\frac{c' \cos\phi' - \sigma_3' \sin\phi'}{c' \cos\phi' - p^{\text{ref}} \sin\phi'}\right)^m \quad \dots (2)$$

Where: E_{50}^{ref} is the reference stiffness modulus for primary loading, typically defined at a reference confining pressure $\sigma_3' = p^{\text{ref}}$; p^{ref}: Reference pressure; c': Effective cohesion; φ': Effective angle of internal friction; σ_3': Effective confining stress; m: Stress dependency parameter. In PLAXIS, a default setting is $p^{\text{ref}} = 100\ kN/m^2$, is used.

The asymptotic shear strength q_a is related to ultimate shear strength q_f through failure ratio $R_f = q_f / q_a$.

The ultimate deviatoric stress, q_f is derived from the Mohr-Coulomb failure criterion based on shear strength parameters c and φ and confining pressure σ_3 as described in Equation 3:

$$q_f = \frac{2c\cos\varphi - 2\sigma_3 \sin\varphi}{1 - \sin\varphi} = (c\cot\varphi - \sigma_3)\frac{2\sin\varphi}{1 - \sin\varphi} \quad \dots (3)$$

The main difference between HSM and the M-C model is the stiffness approach. Here, the soil is described much more accurately by using three different input stiffnesses: triaxial loading stiffness E_{50}, triaxial unloading/reloading stiffness E_{ur}, and the

oedometer loading stiffness E_{oed}. Additionally, adding three input stiffness values can improve the modeling of soil deformation magnitude (Obrzud & Truty, 2018). HSM takes into consideration the stiffness moduli's stress-dependency, which could suggest that stiffnesses rise as earth pressure rises (Laosuwan et al., 2016) as can be noted in Equation 2. In addition, HSM capable to modeling the intense shear dilatancy behaviors of dense granular materials, and uses isotropic strain hardening which can forecast shearing properties in specific situations as addressed by many researchers (Laosuwan et al., 2016; Pramthawee et al., 2011). The stress dependent stiffness modulus for unloading and reloading stress paths is calculated as:

$$E_{ur} = E_{ur}^{\text{ref}} \left(\frac{c' \cos\phi' - \sigma_3' \sin\phi'}{c' \cos\phi' - p^{\text{ref}} \sin\phi'} \right)^{m} \quad \ldots(4)$$

E_{ur}^{ref}: Reference stiffness modulus for primary loading, typically defined at a reference confining pressure $\sigma_3' = p^{\text{ref}}$.

For a practical case, PLAXIS gives the default setting of E_{ur}^{ref} equal to $3E_{50}^{\text{ref}}$.

The shear hardening yield function (*fs*) in the HSM is given as:

$$f_s = \bar{f} - \gamma^p \ldots (5)$$

$$\bar{f} = \frac{q_a}{E_{50}} \left\{ \frac{(\sigma_1' - \sigma_3')}{q_a - (\sigma_1' - \sigma_3')} \right\} - \frac{(\sigma_1' - \sigma_3')}{2E_{ur}} - \gamma^p \ldots (6)$$

where σ_1' and σ_3' are the major and minor effective principal stresses, and γ^p is the plastic shear strain, and can be approximated as

$$\gamma^p \approx \varepsilon_1^p - \varepsilon_2^p - \varepsilon_3^p = 2\varepsilon_1^p - \varepsilon_v^p \approx 2\varepsilon_1^p \ldots (7)$$

Where $\varepsilon_1^p, \varepsilon_2^p, and\ \varepsilon_3^p$ are the plastic strains, and ε_v^p is the plastic volumetric strain.

It can be noted from the formulation of shear hardening yield functions from the Equation 6, the triaxial moduli (E_{50}^{ref} and E_{ur}^{ref}) are parameters that control the shear hardening yield surfaces.

In reality, plastic volumetric strains ε_v^p will never be precisely equal to zero, but for hard soils plastic volume changes tend to be small when compared with the axial strain, so that the approximation in Equation 7 will generally be accurate (Schanz et al., 1999). Shear hardening and cap yield surfaces in the HSM are shown in Fig.1 for *m*= 1, however, the lines are slightly curved for *m* < 1. The second type of hardening model is cap-type yield surface, which accounts for volumetric hardening. This surface is introduced to close the elastic region in the direction of the p-axis in Fig. 1.

While the triaxial modulus largely controls the shear yield surface, the oedometer modulus controls the cap yield surface. The parameter E_{50}^{ref} primarily influences the extent of plastic strains associated with the shear yield surface. Similarly, E_{oed}^{ref} governs the magnitude of plastic strains resulting from the yield cap. In a similar manner to the triaxial moduli, the oedometer modulus (E_{oed}) obeys the stress dependency law:

$$E_{oed} = E_{oed}^{\text{ref}} \left(\frac{c' \cos\phi' - \sigma_1' \sin\phi'}{c' \cos\phi' - p^{\text{ref}} \sin\phi'} \right)^{m} \ldots (8)$$

The cap yield function, f^c, and plastic potential function, g^c, are defined as:

$$f^c = g^c = \frac{q^2}{M^2} + (p - cot\varphi)^2 - (p_c - cot\varphi)^2 \ldots (9)$$

$$q = \sigma_1 + (\propto -1)\sigma_1 - \propto \sigma_3 \ldots (10)$$

$$\alpha = \frac{3+sin\varphi}{3-sin\varphi} \ldots (11)$$

$$p = \frac{\sigma_1+\sigma_2+\sigma_3}{3} \ldots (12)$$

p_c is the isotropic pre-consolidation stress, and the hardening law relating p_c to the volumetric cap strain ε_v^{pc} is:

$$\varepsilon_v^{pc} = \frac{H}{m+1} \left(\frac{p_c}{p^{ref}} \right)^{m+1} \ldots (13)$$

The volumetric cap strain is the plastic volumetric strain in isotropic compression. Both H and M are cap parameters, which relate to E_{oed}^{ref} and K_o^{nc} , respectively. PLAXIS does not adopt them as input parameters. Instead, their relationships can be expressed as: $M = K_o^{nc}$ (by default $K_o^{nc} = 1 - sin\varphi'$); M= E_{oed}^{ref} (by default $E_{oed}^{\text{ref}} = E_{50}^{\text{ref}}$). Fig. 2 shows the shape of the cap yield as an ellipse in the p-q plane which has length $(p_c + cot\varphi)$ on the p-axis and $\alpha\ p_c$ on the q-axis. The cap yield surface expands as a function of the pre-consolidation stress p_c.

3. Previous investigation and laboratory tests

Essentially, the material for the clay core was extracted from large deposits of residuals of weathered rocks from upper and lower Fars formations. It was defined as brown loamy sand with calcium carbonate nodules formed by precipitation of calcareous materials leached from geological formations overlaying the Fars formations (Blanc, 1963a). During construction laboratory tests specified two types of materials used for the core, they were Fat Clay (CH) and Lean Clay (CL). The two types of clays showed similar physical properties, except a higher Atterberg limits for the Fat Clay (CH) to that for the Lean Clay (CL). The relevant lab test data before the construction can be found in (Blanc, 1963a; Davis, 1958) and during the construction in (Blanc, 1963a). The utilized results for this study belong to the laboratory tests performed by (Analyses and Safety Evaluation, Appendix B, 1987). The samples for the core were taken from two shallow test pits excavated along the crest. The tests included Atterberg limits, moisture content, grading, and consolidated undrained triaxial test. The consolidated undrained triaxial test was carried out on six samples, the samples were remolded and compacted to 95% of

the standard ASSHTO density as quoted by (Blanc, 1963a) and allowed for consolidation before testing. Based on a scattered result of triaxial tests a reasonable failure envelope of c = 0, φ = 24° was drawn accordingly. The graphical presentation for the triaxial tests can be found in the elaborated report by (Analyses and Safety Evaluation, Appendix B, 1987), Appendix (B).

4. Laboratory tests

Recent laboratory tests were conducted on soil samples taken from layers at elevations ranging between (480.5-484.5 m) on the dam crest. These samples were taken during the field investigation targeting the dam body following the 12 November 2017 earthquake. The focus on core material reflects its critical role in maintaining the dam's integrity and controlling seepage. Because the samples were not preserved in their natural state, they primarily provided the material needed to remold the soil samples for laboratory tests. Because the in situ conditions of the core samples were unknown, the remolded samples were reconstituted with varying degrees of moisture content and compaction to replicate the realistic conditions. Several standard laboratory tests, outlined in Table 1, were performed. Furthermore, four (4) soil samples were tested for unconfined compressive strength according to ASTM D2166 guidelines. However, preparing the samples at maximum dry density was challenging because achieving this density required significantly lowering the moisture content. This reduction in moisture made it difficult to achieve proper bonding and integration between soil layers within the test mould. As a result, samples were prepared at relatively lower densities, enabling the use of linear regression to estimate the unconfined strength at higher densities, as shown in Fig. 3. Fig. 4 presents the particle size distribution obtained from hydrometer and sieve analysis tests.

1.1. Oedometer Test

As part of this research, laboratory oedometer tests were conducted on three samples representing the clay core soil of the Darbandikhan Dam. Each sample was defined by specific initial and final conditions, including soil moisture content, dry density, void ratio, and degree of saturation at the beginning and end of the test. A summary of these conditions is presented in Table 2. The tangent modulus (i.e.E_{oed}) which characterizes soil stiffness under primary loading (σ_1) when lateral strain is constrained, is stress dependent. For each soil sample, four (4) tangent moduli were calculated for incremental primary loading (i.e. effective axial stress $\sigma_1^{'}$) and three (3) tangent moduli were calculated during unloading/reloading, and the corresponding values for E_{oed}^{ref} are recorded in Table 3. To evaluate the stress dependency of E_{oed}, the logarithm of the tangent modulus values was plotted against the logarithm of normalized effective stress $\sigma_1^{'the}/p_{ref}$ in normal domain. The procedure of finding E_{oed}^{ref} is identical to the one explained for E_{50}^{ref} in the successive section. The reference tangent modulus E_{oed}^{ref} and the stress dependency power m were obtained using linear regression. The inverse logarithm of the intercept of the linear regression line provides tangent modulus at reference pressure (E_{oed}^{ref}) and the slope of the line represents the stress dependency parameter m. The purpose of this analysis is to predict the embankment settlement during various stages of construction, consolidation, and longterm operation after the reservoir has been filled. Fig.5. shows the soil samples S2 and S3 which they represent the soil condition at relatively low density and moisture content are more susceptible to consolidation, as indicated by the steep gradient of the principal vertical effective stress σ'$_1$ versus the void ratio e. Additionally, Fig. 6. shows a low stiffness value ($E_{oed}^{ref} = 2721$ kN/m^2), and high dependency power $(m \cong 0.74)$ which is evidence of a high level of stress dependency of their tangent modulus E_{oed} at early stages. The soil sample S1 represents the soil at an advanced stage of consolidation. The initial state of this sample represents soil that has undergone significant consolidation and has become denser and stiffer. This is reflected in a higher tangent modulus value $\left(E_{oed}^{ref} = 4942\ kPa\right)$ and lower stress dependency parameter $(m \cong 0.51)$ as noted in Fig.3. The lower m value indicates reduced stress dependency, typical for denser soils at advanced consolidation stages. However, for calculation purposes we would prefer to apply linear regression for the three sample moduli which yield an oedometer modulus value $\left(E_{oed}^{ref} = 3320\ kPa\right)$ and power parameter m= *0.66*. The soil samples demonstrate the same density and moisture content once they reach the final consolidation stage and behave similarly, which can be noted in the unloading/reloading stages of the graph in Fig. 5.

Finally, we conclude that:

- Lower density and moisture conditions (S2 and S3) result in greater susceptibility to consolidation and higher stress dependency of soil stiffness.
- Soil at advanced consolidation stages (S1) becomes stiffer and less stress-dependent, as demonstrated by a higher E_{oed}^{ref} and lower m value.
- For fully consolidated samples of identical soil type, the oedometer test demonstrates the same results regardless of the initial

density and moisture content, as noted during the unloading stages of loading.

1.2. Estimation of Reference Secant Modulus E_{50}^{ref}

The safety and evaluation report conducted by Bennie and Partner Consultancy (Analyses and Safety Evaluation, 1987), contains consolidated undrained triaxial test conducted on six samples at different confining pressures. The samples taken from two test pits of shallow depth up to 1.30 m on the dam crest. The graphical relation between deviatoric stress q and axial strain ε_1 was digitized for each sample, and the graph reproduced with EXCEL software. It was difficult to compute secant moduli from the existing actual graphs, because they exhibit irregularities especially at early stages of loading, in addition the measured secant modulus E_{50} represents undrained condition. To overcome these difficulties a 2D numerical model was simulated with PLAXIS using Hardening Soil Model for undrained triaxial condition which resembles the same initial cell pressure σ_{xx}, maximum strain ε_{yy} and the drainage condition of the laboratory samples. The simulation was run for different combination of stiffness moduli and shear strength parameters of friction angle (φ) with the assumption that drained secant modulus is lower than the undrained one. A best-fit agreement has been achieved between the observed and simulated curve for each test which facilitated the measurement of secant modulus. The secant modulus at 50% of deviatoric stress at failure (E_{50}) is the slope of a straight line originating from the initial point of the stress-strain curve at $(\Delta q = 0, \varepsilon_{yy} = 0)$ and intersecting the curve at a point where the deviatoric stress q is equal to 50% of its failure value, see Fig. 7. Fig. 7. Explaining different stiffness moduli in triaxial test. To estimate secant modulus E_{50} at reference confining pressure p^{ref}, Equation 9 was linearized by taking logarithm of both sides as explained below:

E_{50} is related to E_{50}^{ref}, through the following relation,

$$E_{50} = E_{50}^{ref}\left(\frac{c'cos\phi' - \sigma_3' sin\phi'}{c'cos\phi' - p^{ref} sin\phi'}\right)^m \quad (14)$$

Taking the logarithm for both sides, it becomes,

$$\log E_{50} = \log E_{50}^{ref} + m\log\left(\frac{c'cos\phi' - \sigma_3' sin\phi'}{c'cos\phi' - p^{ref} sin\phi'}\right) \quad (15)$$

In which Equation 15 can be put in a more generalized linear relation form of $(y = a + bx)$ and plotted in normal domain as shown in Fig. 8. The inverse logarithm of y-intercept (10^y) represents the secant modulus at reference confining pressure of 100 kPa (E_{50}^{ref}), and the slope of the line is the stress dependency power m. From Equation 10.: For $\sigma_3 = p^{ref}(100\ kPa)$; $x = \log(1) = 0$, $y = \log(E_{50}^{ref})$

$y = 3.5448 + 0.7995\ (0) = 3.5942$

$E_{50}^{ref} = (10)^{3.5448} = 3505.90\ kPa$

Based on the relationship presented in Fig. 8., the regression coefficient m representing the amount of stress level dependency of stiffness is close to 0.80.

We noted that reference secant modulus E_{50}^{ref} is the most sensitive parameter which significantly affecting the best match between the simulated curve and the observed graph. This adheres to the fundamental of HSM model formulation where secant modulus serves as the primary parameter governing shear deformation. The shear strength parameter φ comes in the second order in the term of sensitivity after E_{50}^{ref}. Friction angle value φ significantly affects the ultimate deviatoric stress value. Laboratory-determined parameters are not always directly suitable as input values for numerical models because the behaviour of soil under controlled laboratory conditions may differ from how it is represented in an adapted numerical scheme. It is common practice to adjust or calibrate these parameters to achieve the best agreement between observed (measured in the field or experiments) and modeled (simulation) results. Table 4 represents the original values estimated secant modulus E_{50} and friction angle φ. Fig. 9 (a to d) shows the comparison between the simulated triaxial test using PLAXIS 2D using the calibrated HSM parameters and the observed curves for undrained triaxial test from the report Bennie & Partner, (1987a) (Analyses and Safety Evaluation, Appendix B, 1987).

1.3. Stiffness exponent

The formulation of HS models assumes the same exponent m for four different stiffness moduli, i.e. E_o, E_{50}, E_{ur} and E_{oed}. The oedometer test data analysis showed that the stress-dependent stiffness exponent (m) was **0.74** for primary loading for soil samples S2 and S3 and **0.51** for sample S1. For unloading-reloading conditions, the three soil samples were considered altogether and the exponent value m was 0.51. On the other hand, the undrained triaxial test data from Bennie and Partner (1986) Report indicated ***m*=0.80** as depicted in Fig. 8. The calibrated m value of 0.73 was used for the numerical simulation. (Kempfert & Gebreselassie, 2006) noted that m values for undrained tests are generally higher than those for drained tests. This could explain the higher m values for undrained triaxial tests from Bennie and Partner undrained test records (m=0.80) compared to the (m=0.73) value used in the numerical simulation which essentially represent drained condition.

1.4. Shear strength parameters

The strength of clays, which are fine-grained soils, depends mainly on the friction between the soil particles and the effective stresses applied to them, effective stresses are the stresses that act on the soil particles after subtracting the pore water pressure. The effective cohesion, which is the shear strength of the soil at zero effective normal stress and defined as an apparent attraction between the soil particles, is negligible for most clays. Some clays may exhibit some cohesion due to partial saturation, which causes suction forces due to the water menisci, or cementation effects, which involves chemical bonding between the soil particles (Obrzud & Truty, 2018). Initially, Davis (1958) provided values derived from triaxial tests, where cohesion (c) was noted as **1.1 kg^f/cm^2 (11 kPa)**, and the internal friction angle ϕ was specified as **13^o**. However, Davis did not explicitly mention whether these triaxial tests were conducted under drained or undrained conditions. Subsequent investigation by Bennie and Partners (1986) proposed different values **(c=0, ϕ'=24^o)** based on consolidated undrained triaxial tests. Considering the ambiguity in Davis's triaxial test conditions and recognizing the importance of effective stress analysis, the preference leans toward Bennie and Partner's values. These values are consistent with the effective stress principles, which makes them compatible with HSM twhich requires representations of the effective stress state. Bennie and Partner's friction angle (φ'=24^o) is also in agreement with (Carter & Bentley, 2016) range for intermediate to high plasticity clays (21–26°), compacted to maximum dry density per AASHTO standards. In addition, the numerical simulation suggested the friction angle (φ'=25^o) which aligns with aforementioned guidelines.

5. Indirect Determination of HSM Parameters Based on Correlations

1.5. Un/re-loading Poission's ratio

The initial values of Poisson's ratio for small stress levels are between 0.1 and 0.2 for different types of soils and rocks. Thus, a typical value of 0.2 can be used for the elastic unloading/reloading Poisson's ratio ν_{ur} for most soils for HS model based on the suggestion of (Schanz et al., 1999).

1.6. Estimating Stiffness Moduli from Correlations

Secant and unloading-reloading moduli are stiffness moduli that relate to the stress-strain behavior of cohesive materials. They follow the relation: $E_{50} < E_s < E_{ur}$

The static modulus or secant modulus, E_s, is derived from the initial part of the curve that correlates q (deviator stress) and ε_1 (axial strain) in a triaxial drained compression test at $\varepsilon_1 = 0.1\%$.

If E_{50} or E_{ur} are not available from experimental curves, a reasonable approximation for many practical situations is to use: $\frac{E_{ur}^{ref}}{E_{50}^{ref}}$= 2 to 6 (an average can be assumed equal to 4). However, note that the following condition should be satisfied: $\frac{E_{ur}^{ref}}{E_{50}^{ref}} > 2$.

In the absence of laboratory results, assuming that soil behavior follows the stress-strain relation described by Equation 1 which is related to the Hardening Soil Model, and assuming ε_1 = 0.1%, these moduli can be estimated from experimental Equation 16 which is graphically presented in Fig. 10.

$$E_s = \frac{q}{0.001} = \frac{1}{\frac{1}{2E_s} + \frac{0.001 \cdot R_f}{q_f(\phi,c)}} \dots (16)$$

Based on recent laboratory tests, the core segment of Darbandikhan dam consists of a soil type that resembles ***silty clay (medium plasticity clay)*** with soil consistency ranging from stiff to very stiff. To estimate the moduli for this soil, an average value of the static modulus E_s for the stiff state is considered. According to Table 7, this value is E_s = 10,000 kN/m^2. Using the relation in Fig. 10., the ratio E_s /E_{50} can be obtained for a soil with a friction angle of **φ = 24** degrees and a cohesion of c = 0. The result is $\frac{E_s}{E_{50}}$ = 1.69 (fore σ_3=100 kPa), which leads to $\boldsymbol{E_{50}^{ref}}$ = 10,000/1.69 = **5917** kN/m^2. We may notice the estimated value for $\boldsymbol{E_{50}^{ref}}$ is significantly higher than the measured value from triaxial tests. This emphasize the importance of using verified soil parameters based on laboratory test before using in any subsequent calculations.

1.1. Coefficient of earth pressure at rest

The coefficient of earth pressure at rest, denoted by K_o is the ratio of the horizontal to vertical effective stress in a soil mass that is not deformed. It depends on the soil type, density, and stress history. For normally consolidated soils, K_o can be estimated from the effective friction angle φ' using the well-known Jaky (1944) empirical equation:

$K_o^{NC} = 1 - \sin\phi'$

For $\varphi' = 25'$; $K_o^{nc} = 1 - \sin 25' = 0.577$

6. Discussion

It is important to achieve the correct estimation and calibration of the HSM parameters of the clay core in the Darbandikhan Dam for further enhancement of numerical analyses of the dam. The integration of the available data from previous investigations and laboratory testing with numerical modeling was quite an effective approach to derive the parameters of the

advanced constitutive model of soil. The stress-dependent stiffness of the clay core material, described by the tangent modulus E_{oed}, showed a strong difference in consolidation behavior amongst the three samples tested, as presented in Table 3. Samples S2 and S3, with relatively lower densities and moisture contents, are more prone to consolidation, with higher stress dependency of their stiffness, this is reflected in the relationship between the void ratio and effective stress in Fig 5. While Sample S1, representative of a more advanced stage of consolidation, had higher values of the initial odometer modulus E_{oed} and a lower stress dependency parameter m, it showed the expected behavior for more consolidated and denser soil. All samples tend to converge to similar densities and stiffness values after full consolidation, as shown by their behavior during unloading and reloading cycles. Fig. 5. More information on the strength characteristics of the clay core was obtained from the unconfined compression test results. The average value of q_u is 262.90 kN/m², while the average c_u was 131.45 kN/m² as shown in Table 1. The linear relationship between undrained shear strength and dry density, as indicated in Fig. 3, confirmed that with higher densities, the shear strength increases, reflecting the role of compaction in improving soil behavior. The particle size distribution and hydrometer analysis from Fig. 4 gives the percentage of the particle sizes in the clay core as 42.01% clay, 46.03% silt, and 11.96% sand, thus making it silty clay. The Atterberg limit resulted in a liquid limit value of 40% and a plasticity index of 16%. This classifies this soil into medium to high plasticity soil, which shows the soil to be cohesive and plastic. Further evidence of the sensitivity of E_{50} to soil behavior under shear loading was obtained by its calibration based on undrained triaxial tests. The variation of the secant modulus with confining pressure shown in Fig. 8 indicated a value of the stress dependency parameter m= 0.80, aligning with previous conclusions related to cohesive soils in undrained conditions. The calibrated values of E_{50} derived from PLAXIS in numerical simulations show a good comparison with experimentally observed stress-strain curves obtained from laboratory tests, as shown in Fig. 9 (a to d), validating the reliability of the derived parameters. Another remarkable observation was the difference between the E_{50} estimates derived from the laboratory and correlation-based estimations. For instance, the correlation-based estimation of E_{50} was as high as 5917 kN/m², while the calibrated value used in the simulations was 3100 kN/m². This highlights the need for calibration of the parameters with observed data to avoid overestimation of the soil stiffness which can lead to unrealistic predictions of deformations and stability. The calibrated shear strength parameters c′=0, φ′=25° in very good agreement with historical values as reported by Bennie and Partners 1986 [5]. Friction angle φ′ is highly sensitive to influence ultimate deviatoric stress q_f as obtained from the triaxial test simulations as depicted in Fig. 9. Although the laboratory tests were really informative, reconstituted samples have certain limitations in terms of replicating in-situ conditions such as long-term compaction and moisture states. Such factors may lead to minor discrepancies in the estimation of parameters, especially for properties highly dependent on stress, such as E_{50}. Numerical analysis with calibrated parameters provides an excellent basis for the assessment of the response of the dam under static and seismic loading. Nevertheless, extensions of this methodology to other dam zones, including shell and foundation materials, should be made. Besides, the estimation of these parameters may well benefit from further in-situ testing and geophysical surveys.

7. Conclusion

This paper presents the holistic approach adopted in estimating the soil parameters required for the Hardening Soil Model HSM for the clay core of Darbandikhan Dam. The integration of available data, laboratory testing, and numerical modeling has led to the following key outcomes in this study: Parameters such as E_{50}, E_{50}, and E_{ur} were calibrated and could represent the soil's behavior realistically in numerical analyses. Numerical simulations using PLAXIS were also in good correspondence with the results from laboratory tests and confirmed the validity of the calibrated parameters. Quantification of stress-dependent stiffness and consolidation characteristics was done for the clay core. This illustrated the influence that density and moisture conditions have on settlement and deformation. The relation between undrained shear strength and various degrees of soil density and moisture content. This explained how the degree of compaction, and hence dry density, influences undrained shear strength. Undrained shear strength c_u is important in assessing the soil response to undrained loading conditions, particularly under specific dynamic loading conditions.

The methodology presented in this paper can be referred to for similar studies on other earth dams, especially those in seismic zones, where the determination of deformation caused by seismic activity is quite important. In other words, the presented investigation underlines the refinement of available soil data before its use in advanced models, particularly for those supporting critical infrastructure. Future research should extend this approach to other materials, investigating the effect of different loading conditions on enhancing dam safety evaluations. We recommend performing field investigations such as Cone Penetration Tests (CPT)

and Standard Penetration Tests (SPT) to obtain direct measurements of in-situ soil properties, which are critical for the accurate calibration of soil models and for understanding the actual behavior of the clay core under field conditions. Performing geophysical tests, such as MASW, SASW, cross-hole, or downhole, to estimate soil dynamic properties such as shear stiffness and damping parameters (G_{max}, ζ). However, these tests require specialized equipment, dedicated fieldwork, and expert interpretation, making them a substantial task beyond the current study's scope. Therefore, we suggest addressing this important aspect in future research.

References

Abdullah, W., Rafiq, S. K., & Alshkane, Y. M. (2020). Severity of Damage Due to 2017 Kurdistan Region of Iraq-Iran border Earthquake (Halabja Earthquake). *IOP Conference Series: Materials Science and Engineering*, *978*(1), 012017. https://doi.org/10.1088/1757-899X/978/1/012017

Al-Husseinawi, Y., Li, Z., Clarke, P., & Edwards, S. (2018). Evaluation of the Stability of the Darbandikhan Dam after the 12 November 2017 Mw 7.3 Sarpol-e Zahab (Iran–Iraq Border) Earthquake. *Remote Sensing*, *10*(9), Article 9. https://doi.org/10.3390/rs10091426

AL-Rahal, T. H., Khattab, S. I., & Al- Sulayfani, B. J. (2020). Numerical Investigation the Failure Mechanism of Left Slope of Darbandikhan Dam. *Al-Rafidain Engineering Journal (AREJ)*, *25*(2), 1–11. https://doi.org/10.33899/rengj.2020.126573.1013

Al-Taie, A. J., & Albusoda, B. S. (2019). Earthquake hazard on Iraqi soil: Halabjah earthquake as a case study. *Geodesy and Geodynamics*, *10*(3), 196–204. https://doi.org/10.1016/j.geog.2019.03.004

Analyses and Safety Evaluation. (1987). Bennie & Partner Geotechnical Laboratory.

Analyses and Safety Evaluation, Appendix B. (1987). Bennie & Partner Geotechnical Laboratory.

Blanc, G. J. (1963a). The Derbendi Khan Project: Part One. *WATER POWER*.

Blanc, G. J. (1963b). The Derbendi Khan Project: Part Two. *WATER POWER*.

Carter, M., & Bentley, S. P. (2016). *Soil Properties and their Correlations* (1st ed.). Wiley. https://doi.org/10.1002/9781119130888

Coyne and Bellier. (1978). *Darbandikhan Dam Main Remedial Work-Phase 3* [Design Report- Text and Appendix]. Coyne and Bellier.

CREA Hyrdo & Energy. (2022). *Analysis and safety evaluation of Derbendikhan Dam Final Report-CREA*. CREA Hyrdo & Energy.

Davis, C. V. (1958). Rockfill Dams: The Derbendi Khan Dam. *Journal of the Power Division*, *84*(4), 1741–23. https://doi.org/10.1061/JPWEAM.0000153

Huang, Z., Zhang, G., Shan, X., Gong, W., Zhang, Y., & Li, Y. (2019). Co-Seismic Deformation and Fault Slip Model of the 2017 Mw 7.3 Darbandikhan, Iran–Iraq Earthquake Inferred from D-InSAR Measurements. *Remote Sensing*, *11*(21), 2521. https://doi.org/10.3390/rs11212521

Ibrahim, R., Ghalib A. A., H., Kraft, D. G., & Wang, Y. (in review). Ground Motion Estimation of the Mw 7.3, 2017 Halabja Earthquake. *Seismological Research Letters*.

Kempfert, H.-G., & Gebreselassie, B. (2006). *Excavations and Foundations in Soft Soils*. Springer-Verlag Berlin Heidelberg. https://doi.org/10.1007/3-540-32895-5

Laosuwan, S., Tanchaisawat, T., Department of Civil Engineering, Faculty of Engineering, Chiang Mai University 239 Huay Kaew Road, Muang Distric, Chiang Mai, Thailand, & ,. (2016). Seismic Responses of Zoned Earth-Fill Dam by Instrumentation and Finite Element Simulation. *Journal of Disaster Research*, *11*(6), 1271–1279. https://doi.org/10.20965/jdr.2016.p1271

Mahdi, K. S. (2021). A Review: The Tectonic Perspective and seismic response of Darbandikhan Dam Stability and potential solutions. *IOP Conference Series: Earth and Environmental Science*, *790*(1), 012018. https://doi.org/10.1088/1755-1315/790/1/012018

Mollamahmutoglu, C., & Bedirhanoglu, I. (2019). Investigation of Damage On Derbendikhan Dam During Earthquake Excitation. *Proceedings of International Structural Engineering and Construction*, *6*(1). https://doi.org/10.14455/ISEC.res.2019.199

Naserieh, S., Ghofrani, H., Shoja-Taheri, J., Dezvareh, M., & Mirzaei Alavijeh, H. (2022). Strong Ground-Motion Characteristics Observed in the November 12, 2017, Mw7.3 Sarpol-e Zahab, Iran Earthquake. *Journal of Earthquake Engineering*, *26*(7), 3488–3505. https://doi.org/10.1080/13632469.2020.1806950

Obrzud, R. l F., & Truty, A. (2018). *THE HARDENING SOIL MODEL - A PRACTICAL GUIDEBOOK Z Soil.PC 100701 report revised 21.10.2018* (No. Z Soil.PC 100701 report). Zace Services Ltd, Software engineering. http://www.zsoil.com,

Pramthawee, P., Jongpradist, P., & Kongkitkul, W. (2011). *Evaluation of hardening soil model on numerical simulation of behaviors of high rockfill dams*.

Saed, F. G., Noori, A. M., Kalantar, B., Qader, W. M., & Ueda, N. (2022). Earthquake-Induced Ground Deformation Assessment via Sentinel-1 Radar Aided at Darbandikhan Town. *Journal of Sensors*, *2022*, 1–11. https://doi.org/10.1155/2022/2020069

Salim, S. Gh., & Noori, K. M. G. (2021). Assessment

of the Upstream Slope Stability of Darbandikhan Rockfill Dam during Drawdown. *ARO-THE SCIENTIFIC JOURNAL OF KOYA UNIVERSITY*, *9*(1), 8–15. https://doi.org/10.14500/aro.10678

Schanz, T., Vermeer, P. A., & Bonnier, P. G. (1999). The hardening soil model: Formulation and verification. In *Beyond 2000 in Computational Geotechnics*. Routledge.

Sissakian, V., Sdiq, S., & Haris, G. (2018). Slope Stability of Darbendikhan Dam Site and Near Surroundings. A Reconnaissance Study, Kurdistan Region, NE Iraq. *Journal of Zankoy Sulaimani - Part A*, *20*(3–4), 57–72. https://doi.org/10.17656/jzs.10735

SMEC International Pty. Ltd. (2006, July). *Dokan and Derbendikhan Dam Inspections-World Bank*. www.smec.com.au

Wermelinger, K. (2000). *United Nations Development Programme-Mission Report of Kurt (Dam Engineer)*. COLENCO Power Engineering LTD.

Yaghmaei-Sabegh, S. (2019). Interpretations of ground motion records from the 2017 Mw 7.3 Ezgeleh earthquake in Iran. *Bulletin of Earthquake Engineering*, *17*(1), 55–71. https://doi.org/10.1007/s10518-018-0453-2

Yousif, O. S., Zaidn, K., Alshkane, Y., & Khani, A. (2019, May). Performance of Darbandikhan Dam during a major earthquake on November 12, 2017. *3rd Meeting of EWG Dams and Earthquakes An International Symposium*.

Zaidan, K., Yousif, O. S. Q., Alshkane, Y., Rashed, K. A., & Hama, S. (2021). *Adopted Measures for Evaluation and Remediation of the Damages Occurred in Darbandikhan Dam due toa Major Earthquake*.

تقدير ومعايرة معاملات نموذج تكوينى Hardening Soil Model للتربة المتماسكة باستخدام PLAXIS: دراسة متعلقة بحالة سد دربندخان

المستخلص

تركز هذه الدراسة بشكل أساسي على تحديد ومعايرة معلمات نموذج التربة المسمى Hardening Soil Model لعينات التربة المعاد تشكيلها والتي تمثل اللب الطيني لسد دربنديخان. تم ربط البيانات من التحقيقات السابقة والفحوصات المختبرية بالنمذجة الرقمية لتقدير المعلمات الرئيسية، مثل معاير الصلابة، وأس الصلابة المعتمدة على الإجهاد، ومعلمات مقاومة القص. تم اشتقاق معاملا الصلابة المقطعية E_{50} من اختبارات ثلاثية المحاور المكثفة غير المصرفة عند ضغوط محصورة مختلفة باستخدام PLAXIS بقيمة ٣١٠٠ كيلو نيوتن/م^2. تم تقدير معامل الصلابة E_{oed} من اختبارات التكثيف أحادية البعد عند ظروف مختلفة من الكثافة ومحتوى الرطوبة مما أسفر عن معامل مرجعي قدره ٣٣٢٠ كيلو نيوتن/م^2. تشير النتائج الرئيسية إلى تباين كبير في صلابة التربة وتبعيتها للإجهاد، حيث يتراوح أس الصلابة (m) بين ٠.٦٦ و٠.٨٠، ويتأثر بشدة بالكثافة الأولية ومحتوى الرطوبة. تم معايرة زاوية الاحتكاك (φ) إلى ٢٥ درجة، لتتوافق بشكل وثيق مع البيانات التاريخية. وأخيراً، أظهرت نتائج المحاكاة، المستندة إلى المعلمات المعايرة رقمياً لاختبارات ثلاثية المحاور غير مصفى باستخدام برنامج PLAXIS للعناصر المحدودة، توافقاً قوياً مع النتائج المخبرية.

الكلمات المفتاحية:

معاملات الصلابة للتربة، محاكات أختبار ثلاثية المحاور، نموذج تكوينى للتربة

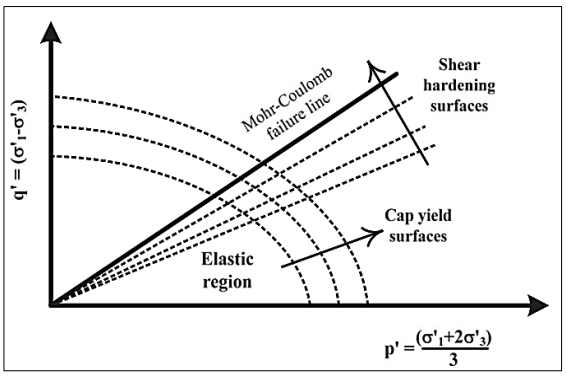

Fig. 1. Shear hardening and cap yield surfaces in the Hardening Soil Model after (Schanz et al., 1999)

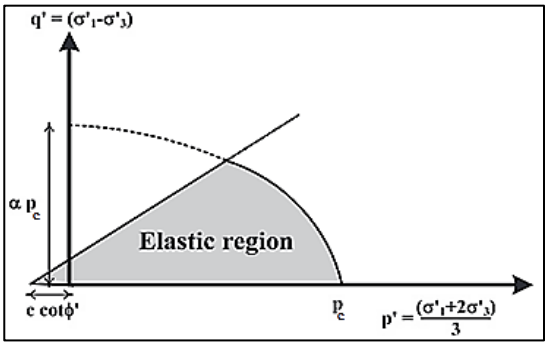

Fig. 2. Cap yield surface in p-q plane

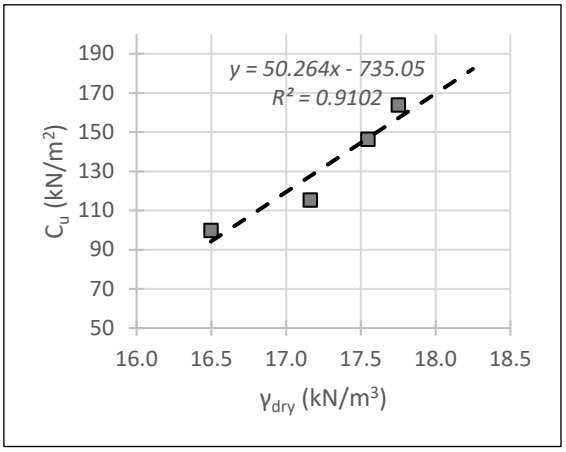

Fig.3. The relationship between undrained shear strength and dry density

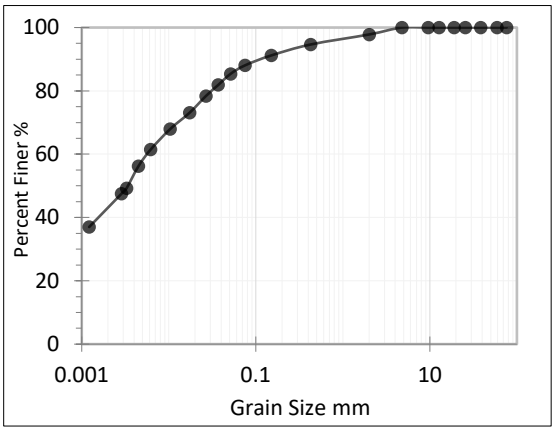

Fig. 4. Particle size gradation for the soil samples taken at elevations

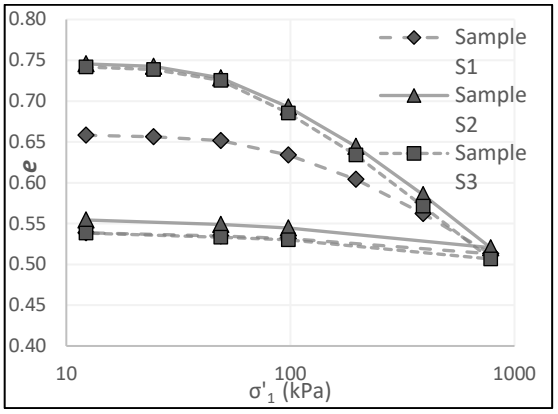

Fig. 5 One dimensional consolidation test (i.e. Oedometer) for clay core samples.

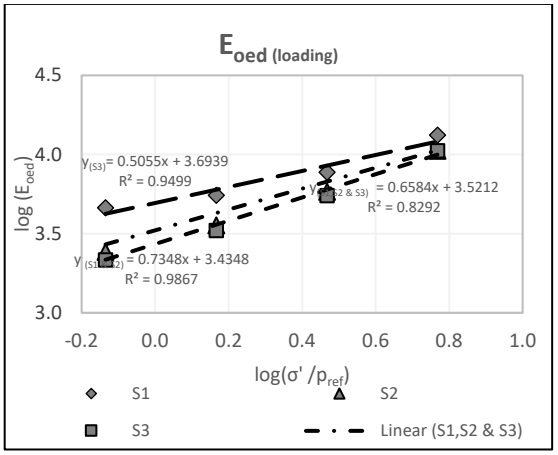

Fig. 6 Relationship between normalized vertical effective stress σ'_1/p_{ref} and E_{oed} at different loading stages

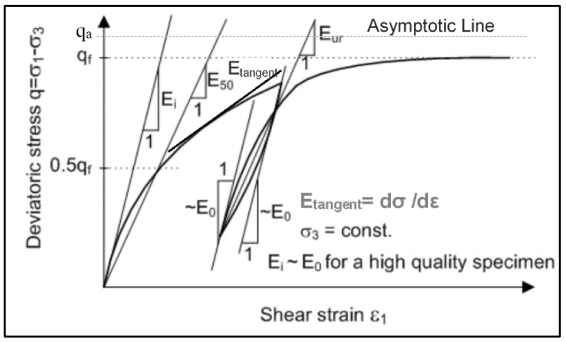

Fig. 7 Illustration of different stiffness moduli from triaxial compression test

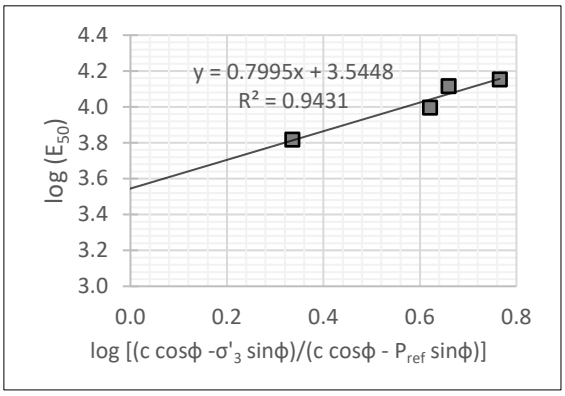

Fig. 8 The relationship between secant modulus E_{50} and confining pressure from consolidated undrained triaxial test for clay

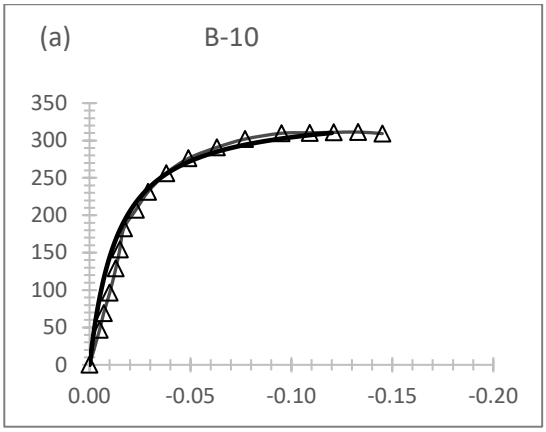

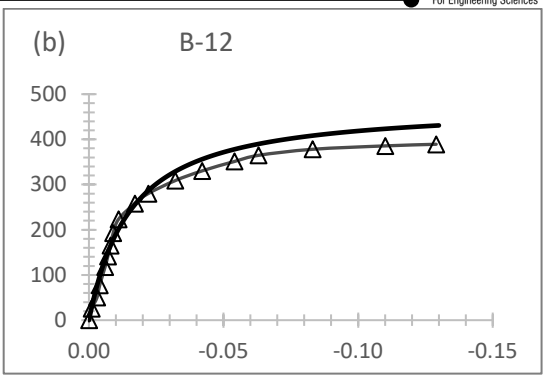

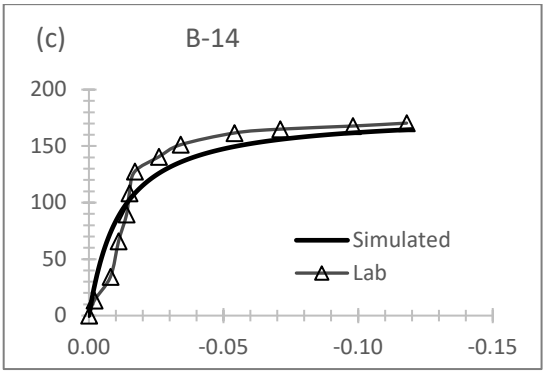

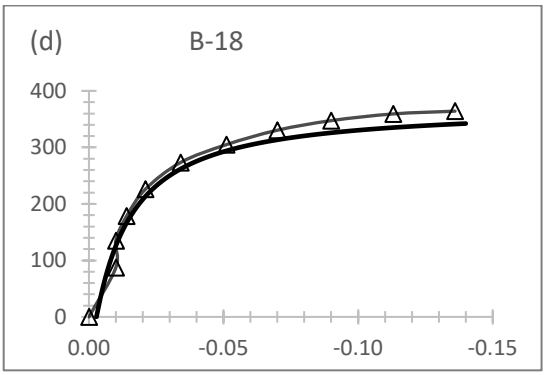

Fig. 9. (a to d) Consolidated undrained triaxial test for Clay core samples and their prediction using Hardening soil model with calibrated soil parameters

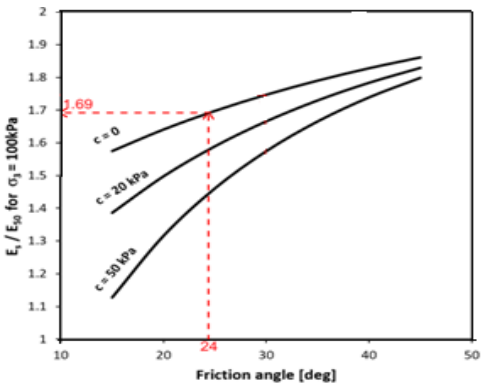

Fig. 10. Estimation of the ratio between static E_s modulus and secant E_{50} modulus

Table 1 Laboratory tests performed on the clay core of Darbandikhan dam

Test	Value		Remark
Maximum Dry Density (kN/m^2)	18.7		Modified AASHTO 2002
Optimum moisture content (%)	13.5		
Atterberg Limits (%)			ASTM D4318
Liquid limit	40		
Plastic limit	24		
Plasticity index	16		
Specific gravity	2.69		ASTM D854
Average Unconfined compression strength q_u (kN/m^2)	262.90		ASTM D2166
Average Unconfined shear strength c_u (kN/m^2)	131.45		
Particle Size and Hydrometer analysis (%)	Sand	11.96	ASTM D422 & D7928
	Silt	46.03	
	Clay	42.01	

Table 2 Condition of clay core sample before and after one dimensional consolidation test

Soli Description	S1	S2	S3
Initial Moisture content (%)	16.5	14.5	12.5
Final Moisture content (%)	18.61	19.35	19.13
Initial void ratio e_o (%)	66.6	75.77	75.25
Final void ratio of (%)	53.15	54.47	53.83
Initial degree of saturation S_o (%)	70.69	53.87	46.75
The final degree of saturation S_o (%)	100.0	100.0	100.0
Initial dry density γ_{di} (gr/cm^3)	1.713	1.602	1.606
Final dry density γ_{df} gr/cm^3)	1.864	1.822	1.829

Table 3 oedometer moduli and stress dependency parameters for core clay samples S1,S2, and S3

Sample ID	E_{oed}^{ref}	$E_{oed(un/re)}^{ref}$	m_{Load}	$m_{(un/re)}$
S1	4942	29345	0.51	0.49
S2	2861	22672	0.71	0.54
S3	2588	26238	0.76	0.50
Avg.	**3464**	**26085**	**0.66**	**0.51**

Table 4 Set of measured and calibrated HSM parameters

Parameters	Parameters measured from laboratory tests	calibrated HS model parameters for clay core
E_{50} (kN/m^2)	3506	3100
E_{oed} (kN/m^2)	3320	3320
E_{ur} (kN/m^2)	14024	12400
m_{oed}	0.66	
$m_{oed\ (ur)}$	0.51	0.73
m_{secant}	0.73	
K_o^{nc}	0.58	0.58
φ (^{o})	24	25
Poisson's Ratio v	…	0.20

Table 5 Typical values for static modulus E_s (MPa) (compiled from Kezdi, 1974; Prat et al.,1995)

Soil Consistency		Silt plasticity		Clay plasticity	
		High	Low	High	Low
Very Soft	Min	2.5	1.5	0.5	0.35
	Max	4	3	3	2
Soft	Min	5	3	2	1.5
	Max	8	6	5	4
Medium	Min	10	6	5	4
	Max	15	10	8	7
Stiff	Min	15	10	8	7
	Max	20	15	12	12
Very Stiff	Min	20	15	12	12
	Max	40	30	30	20
Hard	Min	40	30	30	20
	Max	80	60	70	32